Realization of a Rubidium Atomic Frequency Standard With Short-Term Stability in $10^{-14}\tau^{-1/2}$ Level

Jiaqi Cui, *Member, IEEE*, Gang Ming, Fang Wang, Junyao Li, Pengfei Wang, Songbai Kang, Feng Zhao, Da Zhong, and Ganghua Mei

***Abstract*— Lamp-pumped rubidium atomic frequency standard (RAFS) is one of the most commonly utilized atomic frequency standards. Over the past few decades, the RAFS's frequency stability performance has improved rapidly, and the best one has been in the $10^{-13}\tau^{-1/2}$ level. In this article, we demonstrate an RAFS with stability in the $10^{-14}\tau^{-1/2}$ level for the first time. In design of the physics package (PP), a rubidium spectral lamp with Xe as the starter gas was used as the pumping light source. The light was filtered by using optical and isotope double-filtering technique. A large slotted tube microwave cavity and a rubidium absorption cell with a diameter of 40 mm were utilized to enhance the atomic discrimination signal. A sealed box was designed for the PP to isolate it from the barometric environment. A low phase noise 6.835-GHz microwave was employed to interrogate the rubidium clock transition. Based on the quantitative analysis of the signal-to-noise ratio (SNR) of the atomic discrimination signal and the phase noise of the interrogation microwave, the stability of the RAFS was predicted to be $7.6 \times 10^{-14}\tau^{-1/2}$. The short-term stability of the RAFS was measured by using a hydrogen maser and an optical microwave generator (OMG) as references, and the results are $9.0 \times 10^{-14}\tau^{-1/2}$ (1–100 s) and $9.1 \times 10^{-14}\tau^{-1/2}$ (1–100 s), respectively. The measured results are in agreement with the predicted one.**

***Index Terms*— Environmental effect, interrogation microwave, phase noise, physics package (PP), rubidium atomic frequency standard (RAFS), signal-to-noise ratio (SNR).**

I. Introduction

As ONE of the most widely used atomic frequency standards, the lamp-pumped vapor cell rubidium atomic frequency standard (RAFS) was first developed in the 1960s [1]. In the early 1980s, nearly two decades later, it was commonly recognized that the RAFS had reached its limit in frequency stability performance, the short-term stability may be not better than $1 \times 10^{-11}\tau^{-1/2}$, and the long-term stability, not better than 1×10^{-13} [2]. The situation changed dramatically in the 1990s when the RAFS for GPS block IIR satellites was produced, which is of short-term stability $3 \times 10^{-12}\tau^{-1/2}$ and long-term stability in 10^{-14} level [3]. Furthermore, in the later 2000s, the RAFS for GPS IIM and IIF satellites was reported, its short-term stability reaches $1 \times 10^{-12}\tau^{-1/2}$, and long-term stability is in 10^{-15} level [4].

Our laboratory has been engaged in the development of RAFS for BeiDou navigation satellite system for more than two decades. Since 2007, three-generation RAFSs have been developed. The average performance of the first-generation product is $3 \times 10^{-12}\tau^{-1/2}$ for short-term stability and 4×10^{-14} for one-day stability [5]. The second-generation product has an average performance of $1.5 \times 10^{-12}\tau^{-1/2}$ for short-term stability and 9.4×10^{-15} for one-day stability. The average performance of the third-generation product is $6.1 \times 10^{-13}\tau^{-1/2}$ for short-term stability and 3.9×10^{-15} for one-day stability [6]. In recent years, we have been developing RAFS with even higher stability. Hao et al. [7] designed a desk RAFS system with a stability of $2.4 \times 10^{-13}\tau^{-1/2}$. Nie et al. [8] integrated the system into a whole RAFS unit, and a stability of $2 \times 10^{-13}\tau^{-1/2}$ was achieved. In 2022, we reported an RAFS with a stability of $1.5 \times 10^{-13}\tau^{-1/2}$ [9].

Recently, a new prototype of RAFS was designed in our laboratory. Design work focuses on enhancing the signal-to-noise ratio (SNR) of the atomic discrimination signal, reducing the phase noise of the interrogation microwave, and depressing the environmental effect of the atomic transition. A large size slotted tube microwave cavity and a rubidium absorption cell with 40 mm diameter were designed and utilized to enhance the atomic discrimination signal. Optical and isotope double-filtering technique was used for pumping light to reduce the shot noise of the signal. A low phase noise frequency synthesizer was developed to generate the 6.835-GHz interrogate microwave. To depress the environmental effect, a sealed box was designed to isolate the physics package (PP) from barometric environment. Tests showed that the RAFS is of a short-term stability in $10^{-14}\tau^{-1/2}$ level. In this article, design details and main characteristics of the RAFS are presented and analyzed, and the possible applications of the RAFS are discussed.

Manuscript received 30 September 2023; revised 24 November 2023; accepted 6 December 2023. Date of publication 1 January 2024; date of current version 15 January 2024. The Associate Editor coordinating the review process was Dr. Rosenda Valdes Arencibia. *(Corresponding authors: Da Zhong; Ganghua Mei.)*

Jiaqi Cui and Junyao Li are with the Innovation Academy for Precision Measurement Science and Technology, Chinese Academy of Sciences, Wuhan 430071, China, and also with the University of Chinese Academy of Sciences, Beijing 100049, China (e-mail: baozoudeshuimolin@gmail.com; 542468041@qq.com).

Gang Ming, Fang Wang, Pengfei Wang, Songbai Kang, Feng Zhao, Da Zhong, and Ganghua Mei are with the Innovation Academy for Precision Measurement Science and Technology, Chinese Academy of Sciences, Wuhan 430071, China (e-mail: ming@apm.ac.cn; fang_wang@apm.ac.cn; wpengfei@apm.ac.cn; kangsongbai@apm.ac.cn; zf_lucky@apm.ac.cn; zhongda@apm.ac.cn; mei@apm.ac.cn).

Digital Object Identifier 10.1109/TIM.2023.3348883

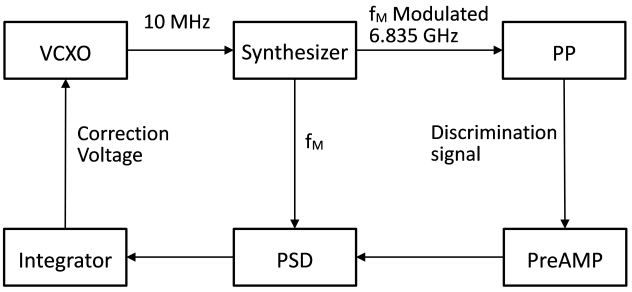

Fig. 1. Block diagram of the RAFS.

II. Structure and Frequency Stability of the RAFS

The electronic structure of the RAFS is shown in Fig. 1. It operates as a frequency-locked loop, utilizing the PP as an atomic frequency discriminator. The reference frequency of the PP is 6.835 GHz, corresponding to the frequency of the transition between hyperfine levels $F = 2$ and $m_F = 0$ and $F = 1$ and $m_F = 0$ of the ground state $5S_{1/2}$ of the ^{87}Rb atom. The transition is also called clock transition. Normally, a 10-MHz voltage-controlled crystal oscillator (VCXO) is used as a local oscillator (LO). The synthesizer converts the 10-MHz signal of the VCXO to a frequency-modulated 6.835-GHz microwave with modulation frequency f_M. The microwave is applied to the PP to interrogate the rubidium clock transition, creating the discrimination signal. After being amplified by the preamplifier (PreAMP), the discrimination signal goes to the phase sensitive detector (PSD) for demodulation, then enters the integrator for filtering and dc amplifying, and finally is transformed into the correction voltage signal to control the frequency of the VCXO, realizing locking of the whole loop.

The SNR of the discrimination signal strongly affects frequency stability which is the key performance of the RAFS. Since the discrimination signal is stimulated by the interrogation microwave provided by the synthesizer, the frequency stability is also influenced by the noise of the microwave. Research showed that the phase noise of the interrogation microwave at $2nf_M$ will deteriorate the frequency stability through the intermodulation effect of the locking loop [10]. In addition, the frequency stability is affected by environmental effects of rubidium atoms. The effects originate from the sensitivity of the atomic transition frequency to fluctuations of various environmental parameters, such as temperature, magnetic field, microwave power, light intensity, barometric pressure, and so on. Taking all the three factors into account, Allan deviation frequency stability of an RAFS can be written as [6]

$$\sigma_y(\tau) = \sqrt{\sigma^2_{\mathrm{SNR}}(\tau) + \sigma^2_{\mathrm{PN}}(\tau) + \sigma^2_{\mathrm{EE}}(\tau)} \tag{1}$$

where τ is the averaging time and

$$\sigma_{\mathrm{SNR}}(\tau) = \frac{\sqrt{S_N}}{\nu_0 K_D \sqrt{2\tau}} \tag{2}$$

$$\sigma_{\mathrm{PN}}(\tau) = \left[\sum_{n=1}^{\infty} C^2_{2n} S_\varphi(2nf_M)\right]^{1/2} \Big/ \tau^{1/2} \tag{3}$$

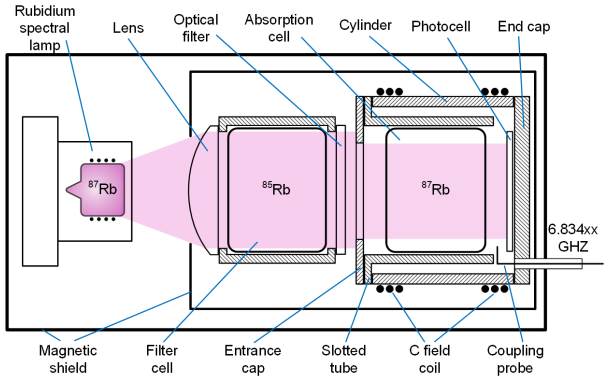

Fig. 2. Structure of the PP.

$$\sigma_{\mathrm{EE}}(\tau) = \sqrt{\sum_i \left(\frac{1}{\nu_0}\frac{\Delta\nu_i}{\Delta P_i}\right)^2 \sigma^2_{pi}(\tau)}. \tag{4}$$

As implied by (1)–(4), three fractional stabilities contribute to the frequency stability of the RAFS. The first one $\sigma_{\mathrm{SNR}}(\tau)$ is SNR limited stability [11], determined by the noise power spectral density S_N and the discrimination slope K_D that measures the signal intensity, where $S_N = 2eI_0$ with e being the electron charge and I_0, the shot noise current [11]. The second one $\sigma_{\mathrm{PN}}(\tau)$ is the phase noise limited stability, determined by $S_\varphi(2nf_M)$, the single sideband power spectral density of the phase noise of the interrogation microwave at $2nf_M$ (C_{2n} is a constant related to the modulation frequency f_M and the carrier frequency been modulated). In the calculation of $\sigma_{\mathrm{PN}}(\tau)$ by using (3), one usually considers only the contribution of the $n = 1$ term, since the contributions of high-order terms are very small [10]. The third one $\sigma_{\mathrm{EE}}(\tau)$ is environmental effect limited stability. In (4), $\Delta\upsilon/\Delta P_i$ and $\sigma_{Pi}(\tau)$ represent the frequency shift coefficient and the stability of the ith environmental parameter P_i, respectively.

It should be noticed that $\sigma_{\mathrm{SNR}}(\tau)$ and $\sigma_{\mathrm{PN}}(\tau)$ determine the short-term stability and the limit of long-term stability of the RAFS, and $\sigma_{\mathrm{EE}}(\tau)$ determines principally the long-term stability. Formulas (1)–(4) also imply that, for the purpose of improving the stability performance of the RAFS, one should focus on enhancing the SNR of the discrimination signal, reducing the phase noise of interrogation microwave, and depressing the environmental effect.

III. Design of the RAFS

A. Physics Package

The atomic discrimination signal originates from a process of optical-microwave double resonance of rubidium atoms that takes place in the PP. Rubidium atoms are first optically pumped by using a rubidium spectral lamp to create population reversion between two clock transition energy levels. Interrogation microwave is then applied to rubidium atoms to stimulate the clock transition. The SNR of the discrimination signal is determined by the characteristics of the PP.

The PP used is schematically shown in Fig. 2. A ^{87}Rb spectral lamp with Xe as starter gas was utilized as the source of pumping light. As shown by Hao et al. [12], this

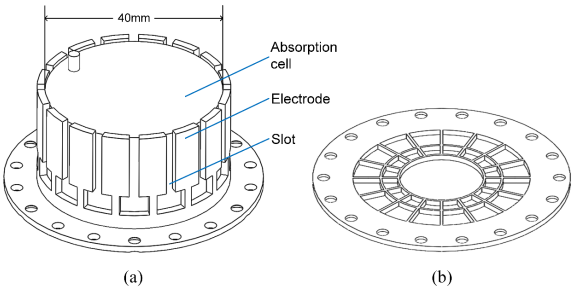

Fig. 3. (a) Slotted tube and (b) entrance cap of the slotted tube microwave cavity.

kind of spectral lump could output intense rubidium D_1 and D_2 line lights with narrow linewidth. After being collimated by the lens, the light is filtered by the ^{85}Rb filter cell to eliminate the *a* components in D_1 and D_2 lines and then filtered by a bandpass optical filter with a center wavelength of 786 nm and bandwidth of 22 nm to eliminate the light emitted by starter gas. This choice of light source and the double-filtering scheme enables to enhance pumping efficiency and meanwhile to reduce the noise of atomic signal. The filtered light then goes to the absorption cell inside a slotted tube microwave cavity composed of a slotted tube, a cylinder, an entrance cap, and an end cap. The absorption cell, with a diameter of 40 mm, contains ^{87}Rb vapor and mixed buffer gases of Ar and N_2. Both the filter cell and the absorption cell were heated and temperature-controlled at appropriate temperatures to create stable and useful rubidium vapors. A modulated 6.835-GHz microwave is electrically coupled into the cavity to interrogate the clock transition of rubidium vapor atoms in the absorption cell. The photocell was used to detect the intensity of the transmitted light through the absorption cell, which varies when the atomic clock transition takes place. A Helmholtz coil produces a uniform *C* field to define quantization axis for atomic transition. Three layers of magnetic shield were employed to reduce the disturbance of environmental magnetic field, two of which were installed on the PP.

The slotted tube cavity is a nonstandard microwave cavity we developed nearly two decades ago [13]. The crucial component of the cavity is a slotted tube, whose structural parameters play main role in determining the resonance frequency and mode of the cavity [14]. An obvious advantage of the cavity over the commonly used standard TE_{111} and TE_{011} cavities is that its size could be flexibly designed. This property enables to use large size absorption cell to enhance the atomic signal SNR. Actually, a series of cavities with different sizes have been developed in our laboratory [5], [6], [7], [8], [9]. In this work, we used the cavity with an inner diameter of 40 mm, the largest one we have designed so far. The structure of the slotted tube is shown in Fig. 3. Fig. 3 also shows the structure of the entrance cap of the cavity, which is needed for a large size slotted tube cavity. The central grid structure of the cap is used to eliminate RF disturbance from outside to resonance mode of the cavity and let pumping light pass through. The entrance cap also acts as an optical aperture to collimate the pumping light into a light beam with a diameter of 32 mm, slightly smaller than that of the absorption cell.

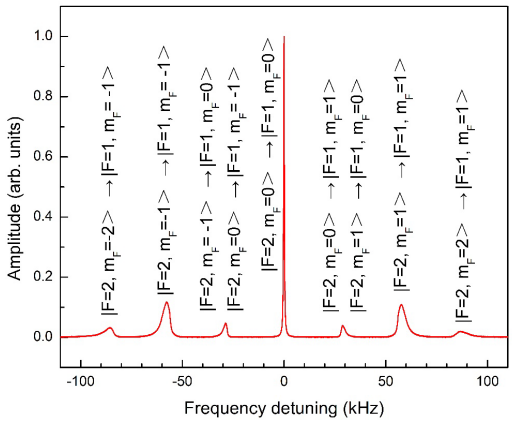

Fig. 4. Zeeman transition spectrum of hyperfine sublevels in ground state of ^{87}Rb atoms. Totally, nine Zeeman transitions were observed. Peak 4 at the center is the clock transition. Peaks 3 and 5 compose of two transitions each.

For high-performance RAFS design, the microwave distribution inside the cavity is extremely important since the clock transition can be excited only by the magnetic microwave field parallel to the quantization axis. The parallelism property is described quantitatively by ξ, the field orientation factor defined as [15]

$$\xi = \frac{\int_V H_z^2 dV}{\int_V |\mathbf{H}|^2 dV} \tag{5}$$

where V defines the volume of interaction region of atoms and microwave, H_z is the magnetic microwave field parallel to quantization axis, and $\mathbf{H}$ is the total field. ξ could be obtained by measuring the Zeeman transition spectrum of ^{87}Rb vapor atoms. The experimentally measured spectrum for the used PP is shown in Fig. 4. Based on the spectrum, ξ could be simply calculated through the relation [16]

$$\xi = \frac{\int I_{4(v)} dv}{\int I_{3(v)} dv + \int I_{4(v)} dv + \int I_{5(v)} dv} \tag{6}$$

where $I_{3(v)}$, $I_{4(v)}$, and $I_{5(v)}$ are the transition intensity distributions of the central three transitions. The finally obtained ξ for the used cavity is 0.82. We believe that it is much higher than those of the traditional standard cavities.

The SNR limited stability $\sigma_{\mathrm{SNR}}(\tau)$ of the PP was estimated. First, the light path and the working temperatures of the absorption cell, the filter cell, and the lamp bulb were optimized for maximum discrimination slope K_d. The optimal temperatures were found to be 68 °C, 93 °C, and 109 °C, respectively. In this condition, the shot noise current I_0, i.e., background current of the photocell, was then measured to be 211 μA, and corresponding noise power spectral density S_N was calculated to be 8.2 pA/Hz$^{1/2}$. Fig. 5 shows the measured frequency discrimination curve of the RAFS. K_d, the slope of the central part of the curve, was calculated to be 18.0 nA/Hz. By using (2), $\sigma_{\mathrm{SNR}}(\tau)$ was estimated to be $4.7 \times 10^{-14}\tau^{-1/2}$, implying that the PP enables to realize a stability in medium $10^{-14}\tau^{-1/2}$ level.

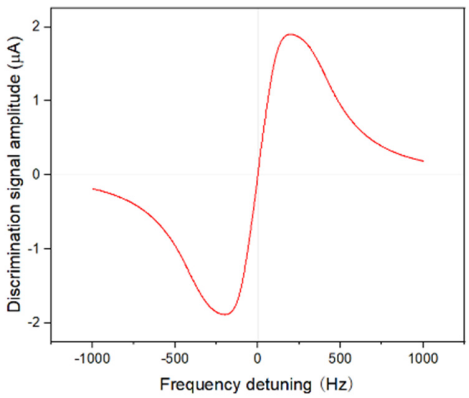

Fig. 5. Frequency discrimination curve of the PP.

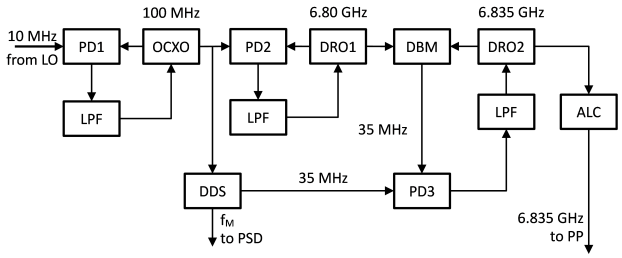

Fig. 6. Schematic of the frequency synthesizer.

B. Frequency Synthesizer

In design of the electronics of the RAFS, main attention was paid to reduce the phase noise and stabilizing the power of the interrogation microwave produced by the synthesizer.

The structure of the synthesizer is schematically shown in Fig. 6. The interrogation microwave originates from a 10-MHz LO with a stability of 1×10^{-12} at 1 s. The 100-MHz frequency of the oven-controlled crystal oscillator (OCXO) with near-end phase noise of -153 dBc/Hz at $2f_M$ (here $f_M = 136$ Hz) is phase-locked to that of the LO through phase detector PD1. Due to the 30-Hz bandwidth of the locking loop, the locked 100-MHz signal is of stability of the LO and the near-end phase noise of the OCXO. For ensuring low phase noise and high spectral purity of the 6.835-GHz microwave, two dielectric resonator oscillators (DROs) with low far-end phase noise are employed, of which DRO1 resonates at 6.80 GHz and DRO2 resonates at 6.835 GHz. The 6.80-GHz frequency of the DRO1 is phase-locked directly to the 100 MHz through PD2. In order to lock the 6.835 GHz of the DRO2 to the 100 MHz also, the frequencies of DRO1 and DRO2 are mixed in the double-balanced mixer (DBM), creating a 35-MHz signal. After being filtered by the low-pass filter (LPF), the 35-MHz signal is phase compared in PD3 with the 35-MHz signal produced by the direct digital synthesizer (DDS) from the 100-MHz signal. The phase comparison signal is then used to control the 6.835-GHz frequency of the DRO2. The finally obtained 6.835-GHz microwave has near-end phase noise property determined by the OCXO, far-end phase noise property determined by the DRO2, and short-term stability property determined by the LO.

The modulation of the 6.835-GHz microwave is realized by modulating the 35-MHz signal of the DDS. The modulation signal is a 136-Hz square wave. The modulated 6.835-GHz microwave is coupled to the PP to interrogate the clock transition of the rubidium atoms.

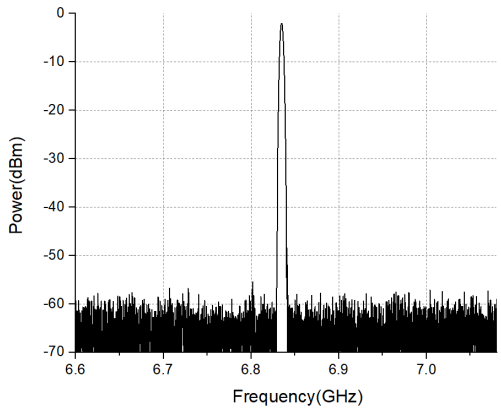

Fig. 7. Spectrum of the 6.835-GHz interrogation microwave.

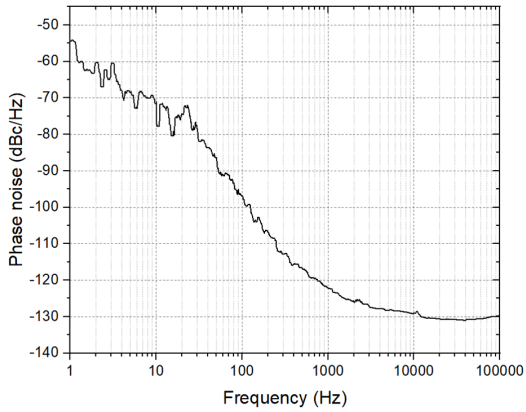

Fig. 8. Phase noise measurement result of the 6.835-GHz microwave.

The interrogation microwave obtained this way is of high spectral purity. As shown in Fig. 7, the output microwave contains only the 6.835-GHz component, and no obvious harmonic or spurious components are observed in a 500-MHz range nearby. In this case, automatic-level control (ALC) of the microwave power will be more efficient since there is less influence of harmonic or spurious components. The stabilization of the microwave power helps to reduce the microwave power shift of the clock transition.

The phase noise of the 6.835-GHz microwave was measured, and the result is shown in Fig. 8. It can be found from Fig. 8 that the phase noise of the microwave at $2f_M$ (272 Hz) is about -110dBc/Hz. Based on this result and by using (4), the phase noise limited stability $\sigma_{\mathrm{PN}}(\tau)$ of the RAFS is estimated to be $6.0 \times 10^{-14}\tau^{-1/2}$.

C. Environmental Effect

As a common sense, for an ordinary RAFS, the influence of environmental effect on short-term stability can be ignored. When an RAFS with $10^{-14}\tau^{-1/2}$ level stability is expected to be realized, however, the influence must be considered.

The first observed unacceptable influence comes from the barometric pressure effect. In our earlier frequency stability measurements of the designed RAFS, the 100-s stability

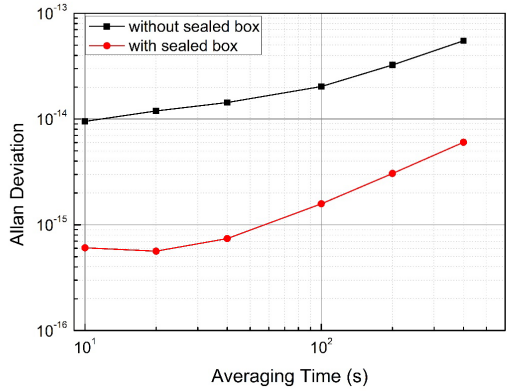

Fig. 9. Influence of the barometric effect to frequency stability of the RAFS.

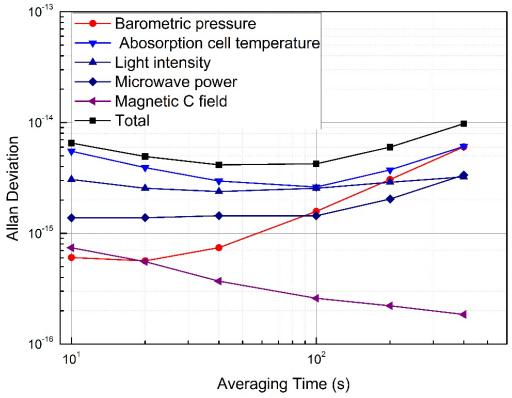

Fig. 10. Contributions of environmental effects to frequency stability of the RAFS. All the results are obtained when the PP is inside the sealed box.

TABLE I
FREQUENCY SHIFT COEFFICIENT OF THE RAFS PHYSICAL PARAMETERS

Physical parameter	Barometric pressure	Absorption cell temperature	Light intensity	Microwave power	Magnetic C field
Frequency shift coefficient	7×10^{-15}/Pa	6×10^{-11}/K	-1.7×10^{-12}/%	6×10^{-14}/%	3.7×10^{-9}/G

was found to be around 2.5×10^{-14} and cannot reach the 10^{-15} level. To make it clear if this is caused by barometric effect, we put the RAFS into a large sealed chamber and measured its frequency shift coefficient of the barometric pressure by changing the air pressure in the chamber and recording the output frequency of the RAFS. The coefficient was experimentally measured to be 7×10^{-15}/Pa. The RAFS was then taken back to the open air environment and the barometric pressure fluctuation was monitored. The barometric pressure was recorded once every 10 s in a period of 50 000 s. Based on the fluctuation data and the obtained frequency shift coefficient, the influence of the barometric effect to stability of the RAFS was calculated by using (4), and the result is shown as the upper line in Fig. 9. The influence to 100-s stability is 2.2×10^{-14}, in agreement with the measured result. To reduce the barometric effect, a sealed box was designed and used to envelop the PP to isolate it from barometric environment. The resulted influence of the barometric effect is shown as the lower line in Fig. 9. It can be seen that the influence is reduced by nearly one order of magnitude. The barometric effect originates essentially from the buffer gas pressure effect inside the absorption cell [17]. Barometric pressure variation deforms slightly the cell shape, thus changes the buffer gas pressure inside the cell and finally causes a frequency shift of the rubidium atomic transition.

The effects of absorption cell temperature, pumping light intensity, 6.835-GHz microwave power, and magnetic C field were also examined in similar way. The frequency shift coefficients of the five parameters are listed in Table I, and the contributions of their fluctuations to the stability of the RAFS with averaging time 10–400 s are shown in Fig. 10.

As can be seen from Fig. 10, all the environmental effects have influences on the stability of the RAFS to some degree. The total influence has been controlled to a 10^{-15} level with $\tau \leq 100$ s, allowing realizing a $10^{-14}\tau^{-1/2}$ level short-term stability. When $\tau > 100$ s, however, the influence increases with τ considerably, which means that the environmental effect will influence the medium-term stability of the RAFS. The influence comes mainly from the temperature shift and the barometric shift, as can be seen from Fig. 10.

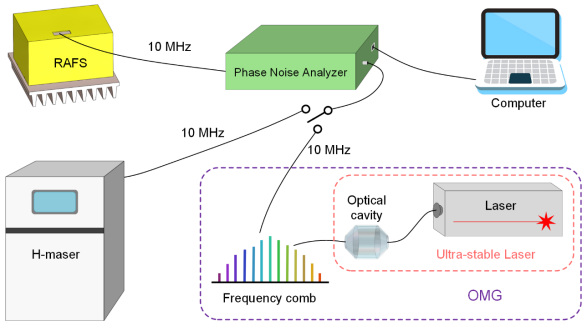

Fig. 11. Frequency stability test scheme for the RAFS. The test could be conducted by using an H-maser or an ultrastable laser based OMG. The phase noise analyzer (3120A, Symmetricom) is used for frequency comparison of the RAFS with the selected reference.

IV. FREQUENCY STABILITY TEST RESULTS

Two references were employed for the frequency stability test of the RAFS. One is a high-performance active hydrogen maser (H-maser) produced by KVARZ (CH1-95), and the other, an ultrastable laser based optical microwave generator (OMG) developed by Qunfeng Chen's group [18]. The test scheme is displayed in Fig. 11.

It should be noticed that, if the tested RAFS and the reference have the same magnitude order of short-term frequency stability, the test result does not reflect the real performance of the RAFS. In this case, the contribution of the reference to the test result should be deducted, and the real stability of the RAFS is then

$$\sigma_{\text{real}}(\tau) = \sqrt{\sigma^2_{\text{test}}(\tau) - \sigma^2_R(\tau)} \tag{7}$$

where $\sigma_{\text{test}}(\tau)$ is the test stability of the RAFS and $\sigma_R(\tau)$ is the stability of the used reference, which is assumed to be known.

The stability result of the RAFS by using the H-maser as the reference is shown in Fig. 12. The result was obtained based on a 5000-s-long frequency data with an averaging time of 1 s. To avoid the influence of frequency drift, the stability performance is given in drift removed Allan deviation. From the circle dot data, the test stability of the RAFS was estimated

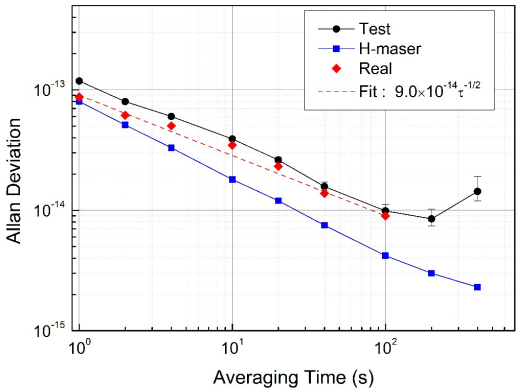

Fig. 12. Frequency stability test result of the RAFS with the H-maser as the reference.

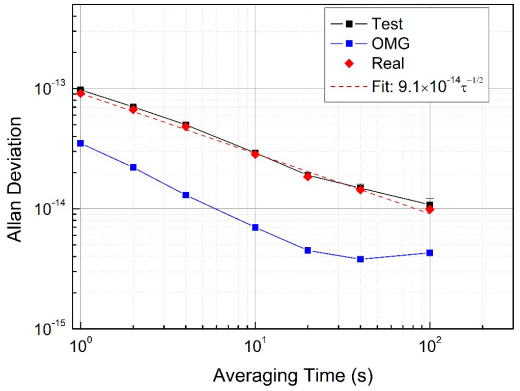

Fig. 13. Frequency stability test result of the RAFS with the OMG as the reference.

to be $1.0 \times 10^{-13}\tau^{-1/2}$ with averaging time τ up to 100 s. The stability goes worse when τ is larger than 100 s; we believe this is caused by the environmental effect (see Fig. 10). By using the test stability data with τ no larger than 100 s and stability data of the H-maser (square dots in Fig. 12), real stability data with τ up to 100 s was obtained (diamond dots in Fig. 12). By fitting the diamond dot data, the real stability of the RAFS was finally obtained to be $9.0 \times 10^{-14}\tau^{-1/2}$ with τ up to 100 s (dashed line in Fig. 12).

Stability result by using the OMG as the reference is shown in Fig. 13. Considering excellent short-term stability but poor medium-term stability of the reference, we give here only the short-term stability result with $\tau \leq 100$ s. As shown in Fig. 13, the test stability of the RAFS is about $9.7 \times 10^{-14}\tau^{-1/2}$, and real stability is calculated to be $9.1 \times 10^{-14}\tau^{-1/2}$ up to 100-s averaging time and strongly supports the result obtained with H-maser.

Based on the SNR limited stability of $4.7 \times 10^{-14}\tau^{-1/2}$ and the phase noise limited stability of $6.0 \times 10^{-14}\tau^{-1/2}$, the stability of the RAFS was predicted to be $7.6 \times 10^{-14}\tau^{-1/2}$. The measured stability result is basically consistent with the predicted one.

V. Conclusion

A lamp-pumped RAFS with short-term stability in $10^{-14}\tau^{-1/2}$ level has been realized. In design of the RAFS, the influences of the SNR of atomic discrimination signal and the phase noise of the interrogation microwave to stability of the RAFS were controlled to $4.7 \times 10^{-14}\tau^{-1/2}$ and $6.0 \times 10^{-14}\tau^{-1/2}$, respectively, and the influence of the environmental effect was controlled to $10^{-15}\tau^{-1/2}$ level. Typical short-term stability of the RAFS reached $9.0 \times 10^{-14}\tau^{-1/2}$ (1–100 s), and symbolizing the vapor cell atomic frequency standard, including the traditional lamp-pumped RAFS and the new generation laser-pumped RAFS, has unprecedentedly achieved a stability in $10^{-14}\tau^{-1/2}$ level. To the best of our knowledge, the previous best result is $1.2 \times 10^{-13}\tau^{-1/2}$, which is realized recently on a pulsed laser-pumped RAFS [19]. The current RAFS device may provide a high-quality oscillator technology, since its 1-s stability has been close to that of the existing best crystal oscillator, while its 10- and 100-s stability and drift performances are much better. If the long-term stability can be improved further, the overall stability of the RAFS will be comparable to that of an active hydrogen maser. Such a compact device can be used as a new generation space clock for satellite navigation system.

Acknowledgment

The authors acknowledge Prof. Qunfeng Chen and his team for providing their OMG device for frequency stability test of the RAFS. They also like to thank Dr. Pengcheng Fang for his helps in the testing process.

References

[1] A. O. McCoubrey, "A survey of atomic frequency standards," *Proc. IEEE*, vol. 54, no. 2, pp. 116–135, Feb. 1966, doi: 10.1109/PROC.1966.4626.

[2] J. Camparo and A. Hudson, "Mesoscopic physics in vapor-cell atomic clocks," in *Proc. Joint Conf. Eur. Freq. Time Forum IEEE Int. Freq. Control Symp. (EFTF/IFCS)*, Besancon, France, Jul. 2017, pp. 47–54, doi: 10.1109/FCS.2017.8088797.

[3] T. B. McCaskill, W. G. Reid, O. J. Oaks, R. L. Beard, J. A. Buisson, and H. E. Warren, "Performance of global positioning system (GPS) on-orbit navstar clocks," in *Proc. IEEE Int. Freq. Control Symp. (49th Annu. Symp.)*, Dana Point, CA, USA, May 1999, pp. 75–89.

[4] R. T. Dupuis, T. J. Lynch, and J. R. Vaccaro, "Rubidium frequency standard for the GPS IIF program and modifications for the RAFS-MOD program," in *Proc. IEEE IFCS*, Honolulu, HI, USA, May 2008, pp. 655–660, doi: 10.1109/FREQ.2008.4623081.

[5] G. Mei et al., "Main features of space Rubidium atomic frequency standard for BeiDou satellites," in *Proc. Eur. Freq. Time Forum (EFTF)*, Apr. 2016, pp. 1–4, doi: 10.1109/EFTF.2016.7477803.

[6] S. Yan et al., "Characteristics of the space-borne Rubidium atomic clocks for the BeiDou III navigation satellite system," *SCIENTIA SINICA Phys., Mechanica Astronomica*, vol. 51, no. 1, Dec. 2020, Art. no. 019512, doi: 10.1360/SSPMA-2020-0245.

[7] Q. Hao, W. Li, S. He, J. Lv, P. Wang, and G. Mei, "A physics package for Rubidium atomic frequency standard with a short-term stability of $2.4 \times 10^{-13}\ \tau^{-1/2}$," *Rev. Sci. Instrum.*, vol. 87, no. 12, Dec. 2016, Art. no. 123111, doi: 10.1063/1.4972567.

[8] S. Nie et al., "A lamp-pumped Rubidium atomic frequency standard with a short-term stability at the level of $2 \times 10^{-13}\ \tau^{-1/2}$," in *Proc. CSNC*, Beijing, China, 2019, pp. 556–563, doi: 10.1007/978-981-13-7751-8_53.

[9] J. Cui, G. Ming, F. Wang, X. Niu, G. Mei, and D. Zhong, "Design and studies of an ultra high-performance physics package for vapor-cell Rubidium atomic clock," in *Proc. CSNC*, Beijing, China, 2022, pp. 403–414, doi: 10.1007/978-981-19-2576-4_36.

[10] C. Audoin, V. Candelier, and N. Diamarcq, "A limit to the frequency stability of passive frequency standards due to an intermodulation effect," *IEEE Trans. Instrum. Meas.*, vol. 40, no. 2, pp. 121–125, Apr. 1991, doi: 10.1109/TIM.1990.1032896.

[11] G. Mileti, J. Q. Deng, F. L. Walls, J. P. Lowe, and R. E. Drullinger, "Recent progress in laser-pumped Rubidium gas-cell frequency standards," in *Proc. IEEE Int. Freq. Control Symp.*, Honolulu, HI, USA, Jun. 1996, pp. 1066–1072, doi: 10.1109/FREQ.1996.560295.

[12] Q. Hao, S. He, F. Xu, F. Zhao, and G. Mei, "Influence of lamp spectral profile on short-term stability and light shift of a Rubidium atomic clock," in *Proc. CSNC*, Xi'an, China, 2015, pp. 387–397, doi: 10.1007/978-3-662-46632-2_34.

[13] G. Mei, D. Zhong, S. An, J. Liu, and X. Huang, "Miniaturized microwave cavity for atomic frequency standard," U.S. Patent US6 225 870 B1, May 1, 2001.

[14] B. Xia, D. Zhong, S. An, and G. Mei, "Characteristics of a novel kind of miniaturized cavity-cell assembly for Rubidium frequency standards," *IEEE Trans. Instrum. Meas.*, vol. 55, no. 3, pp. 1000–1005, Jun. 2006, doi: 10.1109/TIM.2006.873786.

[15] C. Stefanucci et al., "Compact microwave cavity for high performance Rubidium frequency standards," *Rev. Scientific Instrum.*, vol. 83, no. 10, Oct. 2012, Art. no. 104706, doi: 10.1063/1.4759023.

[16] F. Xu, Q. Hao, P. Wang, G. Ming, and G. Mei, "A high signal to noise ratio physics package with a slotted-tube cavity for Rubidium atomic clock," *Acta. Metrologica. Sinica.*, vol. 37, no. 4, pp. 437–440, May 2016, doi: 10.3969/j.issn.1000-1158.2016.04.23.

[17] W. Moreno, M. Pellaton, C. Affolderbach, and G. Mileti, "Barometric effect in vapor-cell atomic clocks," *IEEE Trans. Ultrason., Ferroelectr., Freq. Control*, vol. 65, no. 8, pp. 1500–1503, Aug. 2018, doi: 10.1109/TUFFC.2018.2844020.

[18] R. Xiao, Y. Xu, Y. Wang, H. Sun, and Q. Chen, "Transportable 30 cm optical cavity based ultrastable lasers with beating instability of 2×10^{-16}," *Appl. Phys. B, Lasers Opt.*, vol. 128, Nov. 2022, Art. no. 220, doi: 10.1007/s00340-022-07938-0.

[19] M. Gozzelino et al., "Realization of a pulsed optically pumped RB clock with a frequency stability below 10^{-15}," *Sci. Rep.*, vol. 13, no. 1, Aug. 2023, Art. no. 12974, doi: 10.1038/s41598-023-39942-5.

Jiaqi Cui (Member, IEEE) received the B.S. degree in physics from Wuhan University, Wuhan, China, in 2016. He is currently pursuing the Ph.D. degree with the Innovation Academy for Precision Measurement (APM) Science and Technology, CAS, Wuhan.

His doctoral research study is the enhancement of SNR of physics package of the RAFS.

Gang Ming received the B.S. degree in electronic information from Wuhan University, Wuhan, China, in 2005, and the Ph.D. degree from the Wuhan Institute of Physics and Mathematics (WIPM, former APM), CAS, Wuhan, in 2012.

He is currently a Senior Engineer with APM, CAS. His main research interests include electronics design, parameter optimization, and environmental effect of the RAFS.

Fang Wang received the B.S. degree from Central China Normal University, Wuhan, China, in 2003, and the Ph.D. degree from WIPM, Wuhan, in 2008.

She is currently a Research Professor with APM, CAS, Wuhan. Her main work involves rubidium spectral lamp, lifetime, and reliability of the RAFS.

Junyao Li received the B.S. degree in optoelectronic information engineering from the Huazhong University of Science and Technology, Wuhan, China, in 2016. He is currently pursuing the Ph.D. degree with APM, CAS, Wuhan.

His research work involves barometric effect and frequency drift of the RAFS.

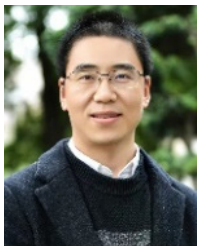

Pengfei Wang received the B.S. degree from the China University of Geosciences, Wuhan, China, in 2009, and the Ph.D. degree from WIPM, CAS, Wuhan, in 2016.

He is currently a Senior Engineer with APM, CAS. His research work involves mainly physics package design for high-performance RAFS and compact RAFS.

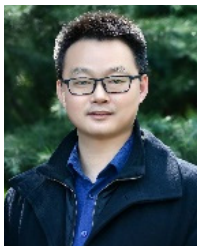

Songbai Kang received the B.S. degree from Wuhan University, Wuhan, China, in 2005, and the Ph.D. degree from WIPM, Wuhan, in 2011.

Afterward, he completed postdoctoral researches with the University of Neuchâtel, Neuchatel, Switzerland, and the National Institute of Standards and Technology, Boulder, CO, USA. He is currently a Research Professor with APM, CAS, Wuhan. His earlier academic interest is in high SNR physics package of the RAFS. His current research interests include traditional and optical RAFS and atomic sensors.

Feng Zhao received the B.S. degree from the Huazhong University of Science and Technology, Wuhan, China, in 2000, and the Ph.D. degree from WIPM, CAS, Wuhan, in 2007.

He is currently a Research Professor with APM, CAS. His earlier work is the design of long lifetime rubidium spectral lamp. His current research interests include physics package design and parameter optimization of the RAFS.

Da Zhong received the B.S. and master's degrees in electronics from Beihang University, Beijing, China, in 1983 and 1988, respectively.

He is currently a Research Professor with APM, CAS, Wuhan, China. Since 1988, he has been engaged in researches on atomic frequency standards, including the passive hydrogen maser and the RAFS. His current interests include high-performance RAFS.

Ganghua Mei received the B.S. and master's degrees in physics from Wuhan University, Wuhan, China, in 1982 and 1985, respectively, and the Ph.D. degree in radio physics from WIPM, CAS, Wuhan, in 1996.

In 1997, he was engaged in researches on the RAFS. As the team head, he led the development of the space RAFS for BeiDou satellites. Since 1998, he has been a Research Professor with WIPM, CAS, and APM, CAS. His earlier academic interests are optical pumping and laser spectrum of atomic beam of alkali and other atoms. His current interests include high-performance RAFS and its applications.